Journal of Photochemistry and Photobiology A: Chemistry 222 (2011) 276–282

Contents lists available at ScienceDirect

Journal of Photochemistry and Photobiology A: Chemistry

journal homepage: www.elsevier.com/locate/jphotochem

Molecular aggregation and photochemical *Z*/*E* isomerization of 1-methy-2-[2-(9-phenantheryl)ethenyl] benzothiazolium iodide

Tarek A. Fayed, Safaa El-Din H. Etaiw*, Mohamed K. Awad, Morad M. El-Hendawy

Chemistry Department, Faculty of Science, Tanta University, 31527-Tanta, Egypt

ARTICLE INFO

Article history:
Received 26 April 2011
Received in revised form 5 June 2011
Accepted 12 June 2011
Available online 16 July 2011

Keywords:
Hemicyanine dye
J-molecular aggregation
Z/*E* photoisomerization
Quantum chemical calculations

ABSTRACT

The steady state absorption and fluorescence spectra of a hemicyanine dye namely, 1-methy-2-[2-(9-phenantheryl)ethenyl] benzothiazolium iodide (9-PhEBI), were measured in different solvents of various polarity including; H_2O, MeOH, EtOH, CH_3CN, CH_2Cl_2 and $CHCl_3$. The photochemical and thermal reactivities were studied in MeOH, EtOH and CH_3CN solvents. The molecular aggregation of 9-PhEBI and formation of J-aggregates was observed in the used solvents even at low concentrations. Further aggregation, with changing the color of the dye from pale yellow to violet, was observed in water. Quantum chemical calculations were employed in order to investigate the intramolecular charge transfer (ICT) process and some quantum chemical parameters. A good agreement between the experimental and theoretical results was found.

1. Introduction

Photochromism refers to a reversible phototransformation of a chemical species between two forms having different absorption spectra. Photochromic compounds change reversibly not only their absorption spectra but also their geometrical and electronic structures [1]. Photochromic materials are potentially useful for various optoelectronic devices such as optical memory, photo-optical switching and display as well as molecular wires. Optical memory using photochromic media offers advantages over magneto-optical recording systems with regard to the speed of writing, multiplex recording capability and low fabrication cost [2]. Efforts have been made to develop erasable compact discs using photochromic diarylethenes [3–5] because they equip most of the necessary properties, particularly, the thermal stability and fatigue resistance [6].

The photochemical *E*–*Z* isomerization about an olefinic double bond is well known example of photochromic reactions. Owing to photoisomerization, azobenzenes, stilbenes, spiropyrans and rhodopsin have been utilized as a trigger or switch to control photochemically various phenomena such as substrate binding of crown ethers [7] or cyclodextrins [8], activity of enzymes [9], permeation of metal ions into liposomal membranes [10] and morphology of synthetic bilayers [11]. In nature, such a photoregulated process is well recognized as a primary stage in the photosynthesis and vision [12].

The structure and spectroscopy of molecular aggregates in which molecules are highly ordered (namely; J- and H-aggregates) are of much interest because of their spectral properties and possible technological applications [13]. This phenomenon plays an important role in biological photosynthesis, in other light-harvesting systems like organic solar cells, and in the photographic industry where the aggregates of dye molecules are used as sensitizer [14]. Briefly, J-aggregates are one-dimensional side by side while the H-aggregates are face-to-face arrangements of molecules [13]. The theory predicts that the strong coupling of several similar monomers in the J- or H-aggregates results in a red or blue shift of their absorption maximum, respectively, relative to the monomer. In addition, the spectrum gets narrower due to the absence of vibrational coupling of the molecular mode.

The photophysics and photochemistry of diarylethenes have been extensively studied by both theoretical and experimental approaches. However, much less is known about that bearing phenanthryl moiety [15–17]. Therefore, 1-methy-2-[2-(9-phenantheryl)ethenyl] benzothiazolium iodide was studied here, Fig. 1. In this context, we have examined the photo-response of this dye in different solvents through the absorption, and fluorescence measurements as well as the photochemical isomerization. Furthermore, its thermo-response has been examined as well. The charge distributions over the whole skeleton, frontier molecular orbitals energies and dipole moment have been calculated using density functional theory (DFT/B3LYP).

* Corresponding author. Tel.: +20 226170229.
E-mail address: safaaetaiw@hotmail.com (S.E.-D.H. Etaiw).

1010-6030/$ – see front matter © 2011 Elsevier B.V. All rights reserved.
doi:10.1016/j.jphotochem.2011.06.008

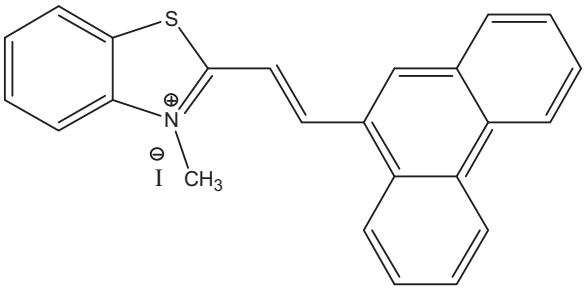

Fig. 1. Molecular structure of 9-PhEBI dye.

2. Experimental and computational details

9-PhEBI was prepared by condensation of 2-methylbenzothiazole with 9-phenanthrylaldehyde according to the general procedure reported for the synthesis of diarylethylenes [18]. Heating of the obtained product, for 1 h under reflux, with equimolar quantity of methyl iodide in ethanol yields 9-PhEBI as a purple amorphous product. It was recrystallized twice from ethanol. The structure was confirmed by elemental analysis, IR and UV–vis spectral measurements. The melting point of 9-PhEBI was 181–183 °C.

Spectroscopic grade MeOH, EtOH, CH_3CN, CH_2Cl_2 and $CHCl_3$ (Aldrich or Merck) were used as received, while water was double distilled. All solvents were found to be non-fluorescent within the range of fluorescence measurements.

Steady-state electronic absorption spectra were recorded on a Shimadzu UV-3101 PC spectrophotometer using 1.0 cm matched silica cells, while the steady-state fluorescence spectra were recorded using a Perkin-Elmer LS 50B scanning spectrofluorometer. Typical concentration of 2×10^{-5} M of the dye was used for the measurements. The fluorescence quantum yields (Φ_f) were determined at room temperature relative to quinine bisulfate in 0.1 N H_2SO_4 (Φ_f = 0.515) [19]. The photoisomerization quantum yields as well as the composition of the photostationary states were calculated as described previously [20]. The light intensity was determined using ferrioxalate actinometry [21].

The thermal $Z \rightarrow E$ isomerization was followed spectrophotometrically. Irradiation was performed at a pre-adjusted temperature (within the range of 15–30 °C) in 3 cm^3 quartz cuvette, containing 3 ml of 3×10^{-5} M of the pure *E*-isomer, using 366 nm light. Irradiation was stopped after reaching the photostationary state, and the sample was moved quickly to a temperature-controlled spectrophotometer cell holder, where the *Z*-isomer starts to isomerize back to the *E*-isomer. The kinetics of this reaction was followed by recording the change in absorbance of the samples at the absorption maximum.

Full geometry optimizations were performed in ground state using density functional theory (DFT/B3LYP) that implemented in Gaussian 03 [22]. However, the optimization, in both ground and excited states, is performed using AM1/CI implemented in MOPAC 7.21 package [23]. We have calculated some quantum chemical parameters such as the charge distributions over the whole skeleton, frontier molecular orbitals energies and dipole moment.

3. Results and discussion

3.1. Molecular aggregation

9-PhEBI hemicyanine dye undergoes molecular aggregation in solution. Since UV–vis spectroscopy is a common technique to study such behavior. The absorption and fluorescence spectra of

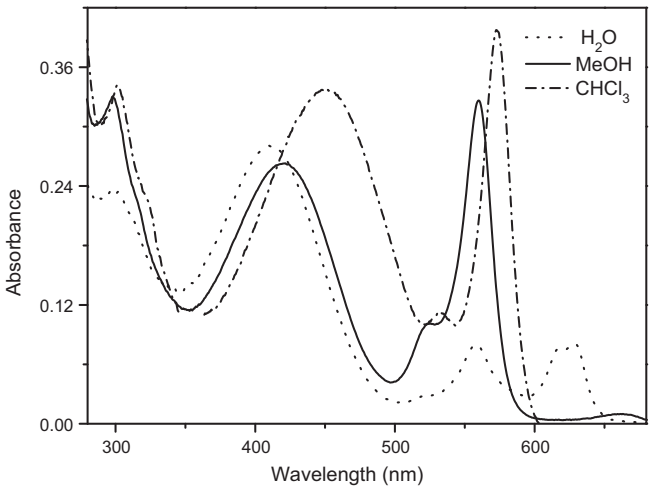

Fig. 2. Absorption spectra of 9-PhBEI in some solvents.

Table 1
Spectroscopic data of 9-PhBEI in various solvents at 25 °C.

Solvent	λ_a^{max} (nm)	ε_{max} (M^{-1} cm^{-1})	*f*	λ_{ex} (nm)	λ_f (nm)
$CHCl_3$	452, 533[sh], 573	14,152, 17,228	0.337	475, 540	527, 591
DCM	449, 526[sh], 566	17,228, 22,273	0.440	467, 531	539, 586
EtOH	425, 526[sh], 563	15,136, 16,982	0.410	464, 530	523, 583
MeCN	413, 522[sh], 562	17,290, 16,367	0.491	462, 528	531, 583
MeOH	422, 533[sh], 560	14,582, 16,613	0.364	462, 529	524, 583
H_2O	410, 558, 625[a]	–	–	461	531, 576

[a] Peak maximum of further aggregation in aqueous solution with color change.

9-PhEBI were recorded in solvents of different polarity, such as H_2O, MeOH, EtOH, CH_3CN, CH_2Cl_2 and $CHCl_3$, in order to investigate the nature of the formed aggregates and the solute solvent interactions. The absorption spectra of 9-PhEBI exhibit two absorption bands around 430 and 565 nm, in addition to a third band around 300 nm, in MeOH, Fig. 2. The higher energy band is broader and more sensitive to the solvent polarity than the lower energy band, Table 1. For example, a blue shift by 42 nm has been induced for the band at 430 nm on going from H_2O to $CHCl_3$. On the other hand, the band at 565 nm is narrow and suffers relatively small blue shift on going from MeOH to $CHCl_3$ (*ca.* 13 nm). It is worthy to mention that both absorption bands appear in the mentioned solvents even at low concentrations ($\approx 10^{-6}$ M). Based on the shape and position of these absorption bands, the lower energy band can be assigned to the formation of molecular aggregates of the J-type [24]. Self association of the ethylene bromide analogue of 9-PhEBI in water and aqueous micellar solutions has been reported [25]. However, the long-wavelength absorption band (around 620 nm) was assigned to the dimmer formation which is not consistent with the used relatively higher concentrations, 100 μM (compared to those used in the present work).

To support this conclusion, the effect of concentration of the dye on the absorption spectrum in MeOH was investigated. Upon changing the concentration of 9-PhEBI from 4×10^{-6} to 8×10^{-5} M, the absorption spectrum displays detectable changes as shown in Fig. 3, where the ratio of absorbance at the two-absorption maxima (A_{560}/A_{421}) increases with increasing the concentration until leveling off at 2×10^{-5} M, within the experimental error, Fig. 4. This indicates growth of the band due to J-aggregates on the expense of the monomeric band at relatively higher concentrations. In addition, the formation of molecular aggregate is explored by checking the linearity of the Beer's law, where negative deviation was observed at both of the two absorption maxima at higher concentrations. However, anomalous behavior was observed in water,

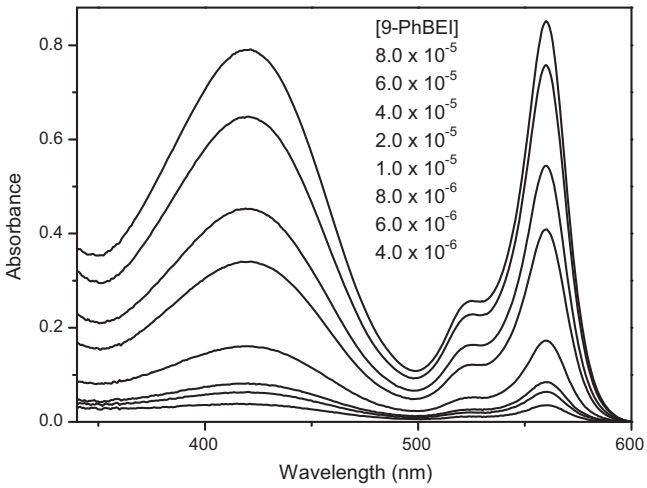

Fig. 3. Effect of the concentration on the absorption spectrum of 9-PhBEI in MeOH.

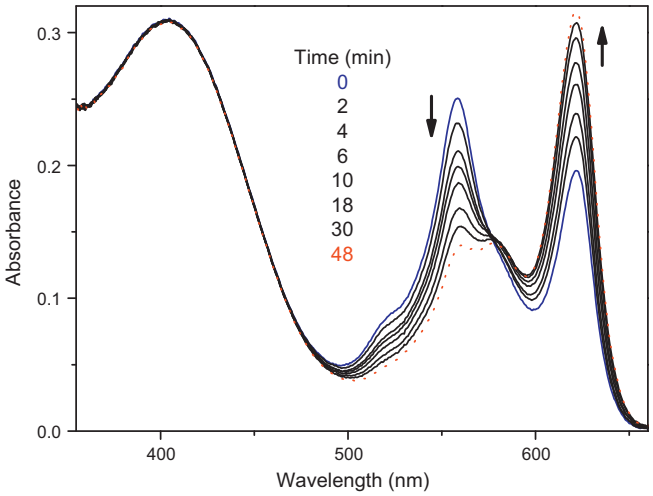

Fig. 5. Variation of the absorption spectrum of freshly prepared aqueous solution of 9-PhBEI with time.

where in addition to the appearance of an absorption band around 560 nm corresponding to formation of the J-aggregates, an additional band was observed at 620 nm. In fact, the color of the fresh solution is red but changes into greenish blue after about 15 min. Therefore, the change in the absorption spectrum of 9-PhEBI in water was monitored as a function of time, Fig. 5. As can be seen, the absorbance of the maximum at 620 nm increases with inherent decrease in the maximum absorbance at 560 nm, and a clear isosbestic point appears at 578 nm with freezing the monomer band. This suggests that higher molecular aggregates are taking places in water because water is the most favorable solvent for the dye aggregation due to its high dielectric constant which reduces the repulsive force between the similarly charged dye molecules in the aggregate. In addition, 9-PhEBI dye is not completely soluble in water and adsorbs strongly from aqueous solutions on the glassware on standing for long (actually, this does not interfere with spectral measurements). This behavior along with absorption in the visible and near-infrared region is technologically important especially for sensitization in photographic industry [26].

Also, the fluorescence behavior of 9-PhEBI has been studied. 9-PhEBI displays dual fluorescence emission when excited at 450 nm in each of the used solvents, Fig. 6. According to the fore mentioned results, the band around 523–540 nm is assigned to the fluorescence of monomeric 9-PhEBI while the shoulder around 575–590 nm is due to fluorescence from the J-aggregates. This was confirmed by recording the fluorescence spectra of 9-PhEBI while the sample was excited at 520 nm, where a high intense and narrower band around 585 nm was mainly observed. It seems that the electronic structure of the monomeric 9-PhEBI is different somewhat from that of the formed aggregates in the excited state. This can be concluded from the different solvent effects on both fluorescence maxima. As shown from Table 1, the emission maximum of the J-aggregates undergoes blue shift with increasing the solvent polarity while that of the monomer is feebly sensitive to the solvent polarity. This is in agreement with the decrease of the dipole moment of 9-PhEBI upon excitation (*vide infra*).

The appearance of two different excitation bands when the excitation spectrum of 9-PhEBI has been recorded at λ_f = 520 and 600 nm, as illustrated in Fig. 7, reflects the presence of two different species in the ground state. The excitation spectrum monitored at λ_f = 600 nm nearly coincides the low energy absorption band indicating that their origin is due to aggregate formation where the vibrational coupling is absent. However, the excitation spectrum recorded at λ_f = 520 nm shows a hint of structure and is blue shifted relative to the broad absorption band.

The total fluorescence quantum yield (Φ_f) of 9-PhEBI was determined in the used solvents and the values are collected in Table 2. The Φ_f values are relatively small and increases noticeably with increasing the solvent polarity (expressed as Kosower's *Z*-parameter [27]) in non-chlorinated solvents. The *Z*-parameter is an empirical parameter corresponding to the CT absorption band

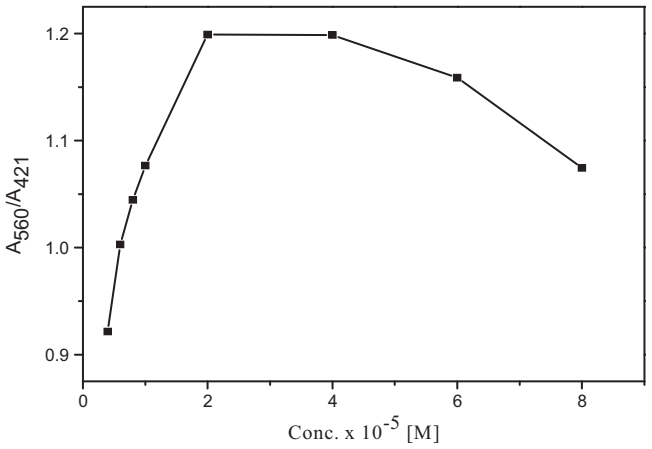

Fig. 4. Dependence of the relative absorbances of the two absorption maxima on the concentration of PhBEI dye in MeOH.

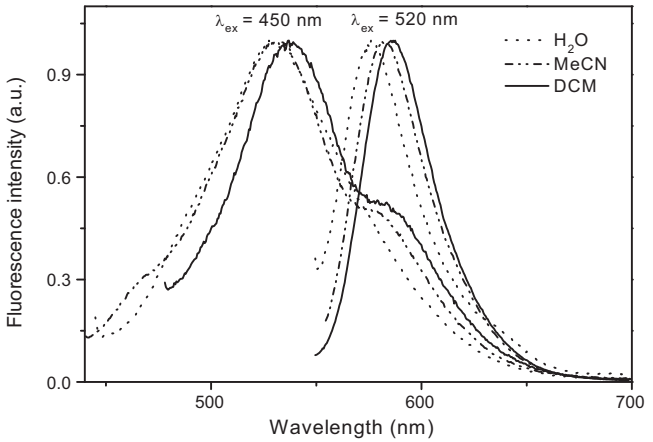

Fig. 6. Normalized fluorescence spectra of 9-PhBEI in some solvents upon excitation at 450 and 520 nm.

Table 2
A list of solvents, the corresponding polarity parameter (*Z*-value), $\Delta\bar{\upsilon}_{st}$ (cm^{-1}) and Φ_f of 9-PhBEI.

Solvent	*Z*-Value	$\Delta\bar{\upsilon}_{st}$ (cm^{-1})		Φ_f
$CHCl_3$	63.2	3149	532	0.034
DCM	64.7	3719	603	0.034
EtOH	79.6	4409	609	0.024
MeCN	71.0	5381	641	0.021
MeOH	83.6	4613	704	0.064
H_2O	94.6	5558	560	0.018

of 1-ethyl-4-(methoxycarbonyl)-pyridinium iodide. The lower Φ_f-values can be attributed to the non planar geometry of 9-PhEBI molecules and the intramolecular charge transfer interaction which enhances the non radiative deactivation of the excited singlet state. In the case of H_2O, the fluorescence yield decreases to 0.018 compared to 0.064 in MeOH, which can be attributed to the formation of additional non-fluorescent high aggregates.

3.2. Direct $E \rightarrow Z$ photoisomerization

The photochemical *E*–*Z* isomerization of 9-PhEBI dye was investigated at room temperature in MeOH only as illustrated in Fig. 8.

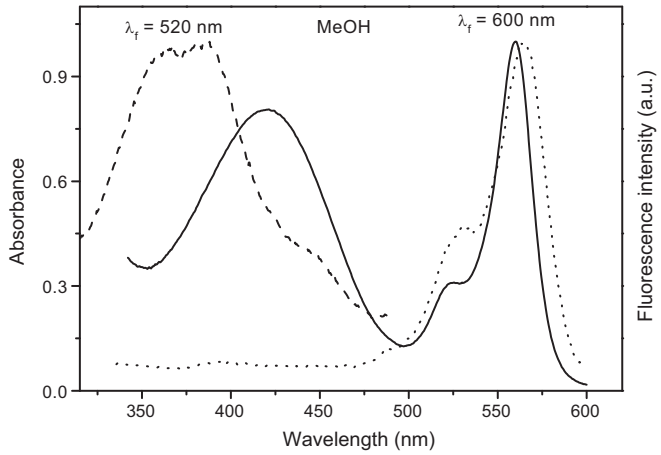

Fig. 7. Electronic absorption (solid) and excitation spectra of 9-PhBEI at λ_f = 520 nm (dash) and 600 nm (dot) in MeOH.

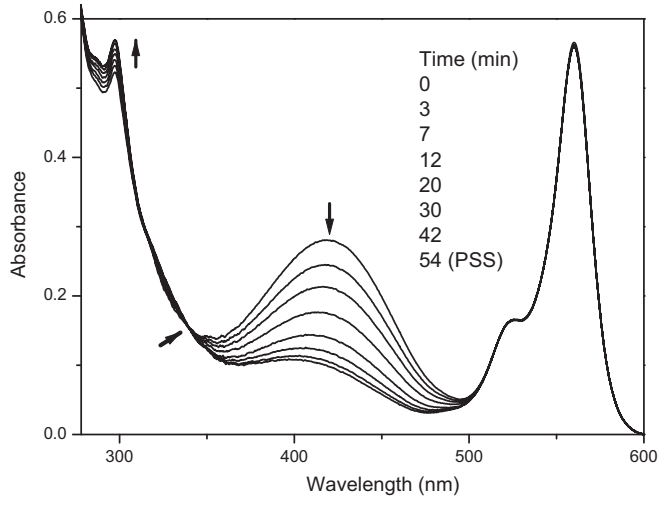

Fig. 8. Effect of photo-irradiation at 436 nm on the absorption spectra of 2×10^{-5} M 9-PhBE in MeOH; the irradiation times at decreasing the absorbance around 422 nm are indicated in the figure.

Table 3
Photochemical data for the $E \rightarrow Z$ photoisomerization 9-PhBEI in MeOH.

405 nm			436 nm		
% *Z*	$\Phi_{E\rightarrow Z}$	$\Phi_{Z\rightarrow E}$	% *Z*	$\Phi_{E\rightarrow Z}$	$\Phi_{Z\rightarrow E}$
89.0	0.329	0.121	92.0	0.273	0.113

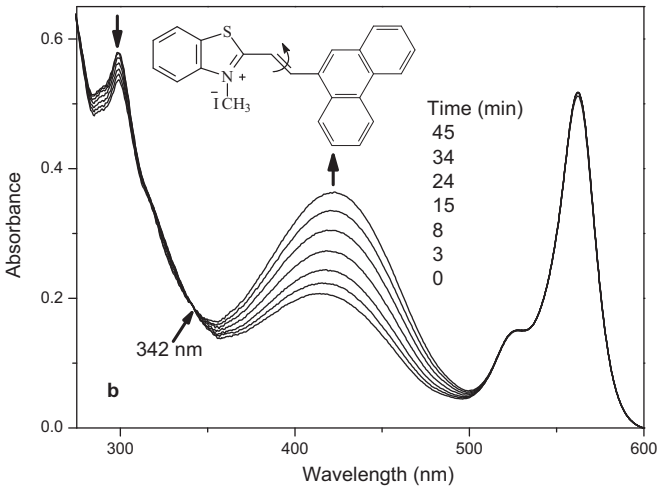

Fig. 9. Change in the absorption spectra of a photostationary state of 9-PhBEI in MeCN at 25 °C; the heating times are indicated.

This is due to the fast backward thermal $Z \rightarrow E$ isomerization of the irradiated solution in other solvents like EtOH and MeCN which does not allow following the photoreaction under steady-state conditions, and the formation of further aggregates in water as discussed previously. Upon irradiation of methanolic solution of 9-PhEBI at 436 nm, the absorbance at the maximum at 422 nm decreases gradually as the irradiation time proceeds, until reaching a constant value confirming the achievement of photostationary state (PSS). This is accompanied by an increase in the absorbance around 299 nm and appearance of an isosbestic point at 339 nm. This reflects the uniform of the photochemical *E*/*Z* isomerization reaction. The composition of the photostationary state (%*Z*) was calculated and found to increase as the irradiation wavelength changes from 405 to 436 nm, Table 3. Meanwhile, the photochemical quantum yields ($\Phi_{E\rightarrow Z}$ and $\Phi_{Z\rightarrow E}$) decrease slightly.

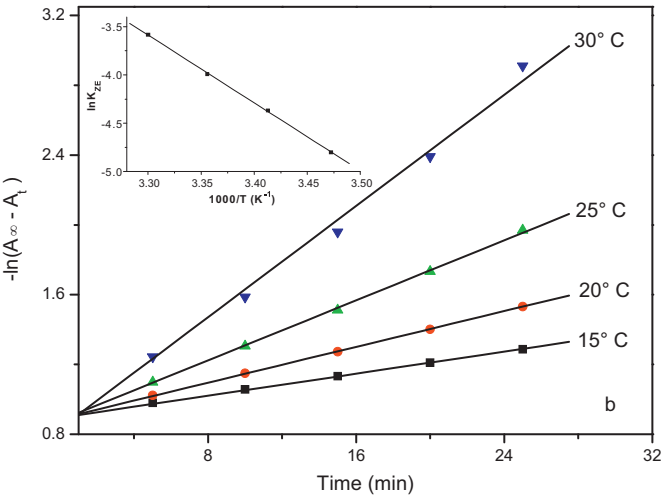

Fig. 10. First-order plots for the thermal $Z \rightarrow E$ isomerization of 9-PhBEI in MeCN at the indicated temperatures; inset: Arrhenius plot.

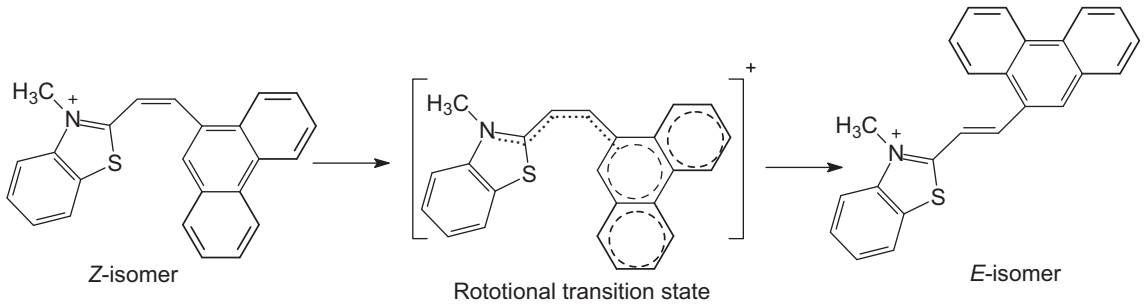

Fig. 11. The rotational mechanism of the thermal $Z \rightarrow E$ isomerization of 9-PhEBI.

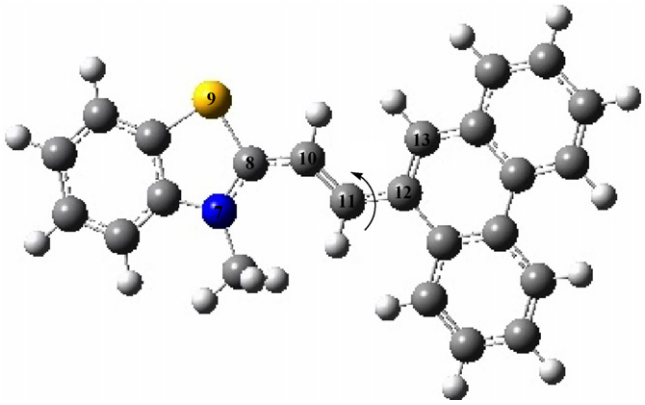

Fig. 12. B3LYP/6-31G(d,p) optimzed geometry of 9-PhBEI molecule.

3.3. Thermal $Z \rightarrow E$ isomerization

The *Z*-isomer of 9-PhEBI dye was found to exhibit back thermal $Z \rightarrow E$ isomerization in MeCN, MeOH and EtOH solvents. However, in other solvents, this hemicyanine dye is either photochemically stable or the thermal reaction is superimposed on the photochemical one. At a given temperature, the gradual change in the absorbance of the photostationary state during the thermal $Z \rightarrow E$ isomerization of PhBEI was monitored spectrophotometrically at the absorption maximum. Fig. 9 shows the thermal isomerization of the *Z*-isomer of 9-PhEBI in MeCN at 25 °C as a representative example. The absorbance of the photostable band at 562 nm does not change during the thermal reaction, while the absorbance of the band at 424 nm enhances continuously as the heating time is increased. The appearance of the isosbestic point at 342 nm confirms the occurrence of a clean thermal conversion between the two isomers. The non-response of longer wavelength band during the photo- and thermal reaction is attributed to the formed molecular aggregate.

The rate constant ($k_{Z \rightarrow E}$) was calculated from the plots, Fig. 10, by applying the first order kinetics, while the activation parameters of the thermal reaction were calculated from temperature dependence of the rate constant, Table 4. The data reveal that, as the solvent polarity increases the rate of the thermal *Z*–*E* conversion decreases which is in agreement with the observed increase in the activation energy, $\Delta E^{\#}$. The observed solvent effect on the $k_{Z \rightarrow E}$ suggests that the thermal isomerization of 9-PhEBI proceeds via a rotation process around the ethenic bridge, Fig. 11, similar to that reported for azobenzenes [28]. It is worthwhile to note that the ICT interaction enhances the single bond character of the central ethenic bridge, which facilitates the rotation process and the thermal $Z \rightarrow E$ isomerization.

The isokinetic relationship (correlation between $\Delta H^{\#}$ and $\Delta S^{\#}$) for the thermal isomerization of 9-PhEBI in different solvents is linear with a good correlation coefficient ($r = 0.92$, plot not shown) from which the isokinetic temperature was calculated (152 °C). At this temperature, the thermal $Z \rightarrow E$ isomerization of the dye follows the same mechanism in the different solvents [29]. However, it was found that the isokinetic temperature is higher than the average of the experimental value, 22.5 °C, reflecting that this reaction is enthalpy controlled [29].

3.4. Quantum chemical calculation

Full geometry optimizations using density functional theory (DFT/B3LYP) showed that 9-PhEBI has a slightly twisted structure, with a dihedral angle C_{10}–C_{11}–C_{12}–C_{13} equals 15° (the angle between ethenic plane and phenanthryl plane as shown in Fig. 12). Based on the DFT-optimized geometry, the structure is re-optimized using AM1/CI producing a similar twisted structure with a dihedral angle equals 21°. Upon excitation using AM1/CI method, the angle is twisted more to 30°.

Quantum chemical calculations using AM1/CI can explore the direction of ICT via two ways; the first one is the distribution of charges on the individual molecular subunits (i.e. phenanthryl, ethenyl and benzothiazolium) in both ground and excited states, which reveals that 81.9% of the net positive charge is carried by the benzothiazolium part in the ground state versus 63.29% in the excited state. This is accompanied by a great charge deficiency on the phenanthryl moiety from 24.59% to 36.72% upon excitation. Accordingly, the benzothiazolium part is regarded as a strong electron acceptor, while the phenanthryl moiety can be considered as a donor. This result agrees with the large decrease in the dipole moment 9-PhEBI from 10.06 to 2.38 Debye upon excitation, which supports our interpretation of the blue shifted absorption spectra of the dye in highly polar solvents.

Besides charge distribution, the orbital topologies could also provide qualitative information about the nature of charge transfer for such D–π–A system. It is shown from the configuration interaction calculations (AM1/CI) that the $S_0 \rightarrow S_1$ transition of the dye has more than 93% of the HOMO–LUMO character. The spatial distri-

Table 4
Rate constant ($k_{Z \rightarrow E}$) of the $Z \rightarrow E$ thermal isomerization of 9-PhBEI (at 25 °C), activation parameters and frequency factor in different solvents.

Solvent	$k_{Z \rightarrow E}$ (min^{-1})	$t_{1/2}$ (min)	$\Delta E^{\#}$ (kJ/mol)	$\Delta H^{\#}$ (kJ/mol)	$\Delta G^{\#}$ (kJ/mol)	$\Delta S^{\#}$ (J/mol K)	A (min^{-1})
EtOH	0.8951	0.77	47.4	45.0	72.8	−94.1	1.7×10^{8}
MeCN	0.0430	16.12	71.0	75.5	80.3	−16.2	2.2×10^{12}
MeOH	0.0024	284.08	73.1	70.6	87.4	−56.8	4.8×10^{5}

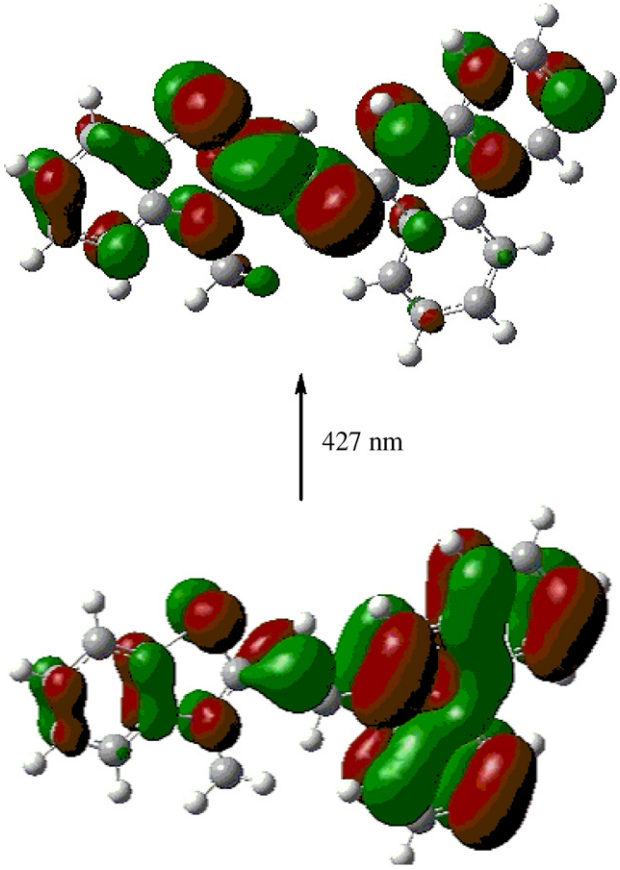

Fig. 13. Visualization of HOMO and LUMO of 9-PhEBI molecule.

bution of the HOMO is highly localized at the phenanthryl subunit while that of LUMO is drifted toward the benzothiazolium moiety, as illustrated in Fig. 13. This reflects that the ICT comes from the phenanthryl subunit to benzothiazolium one via the ethylenic bridge.

The potential energy curves of the ground and lowest excited singlet as a function of the twist angle around the central double bond were calculated using AM1/CI in MeOH, Fig. 14. The energy barrier hindering the internal rotation in the ground state is too high to be overcome in the *E–Z* thermal isomerization (20 kcal). This is consistent with the experimental observation where the *E*-isomer is thermally stable in absence of light. In the ground state the most stable conformation of the *Z*-isomer involves a twisting angle about 40° which seems to be realistic due to the steric hindrance between the hydrogen atoms of ethenyl and phenanthryl moieties, Fig. 14.

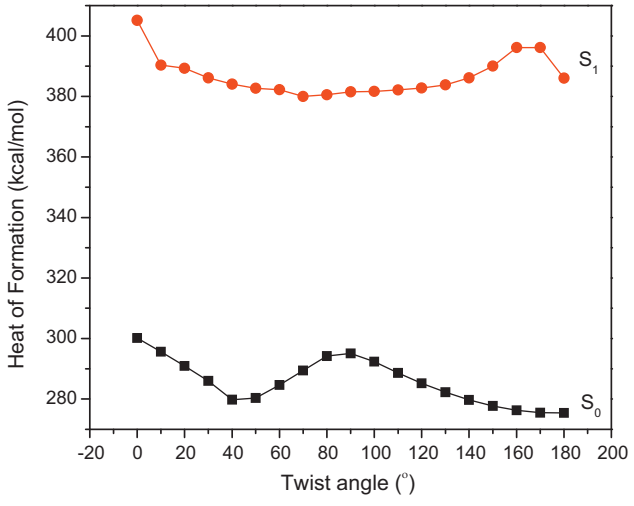

Fig. 14. The potential energy curves of the ground (S_0) and the lowest excited singlet (S_1) states as a function of the twisted angle around the central double bond.

4. Conclusion

In this work, a hemicyanine dye (9-PhEBI) has been synthesized and investigated spectrophotometrically and theoretically. In this context, the absorption and fluorescence spectra of the dye in solvent of various polarities have been recorded. 9-PhEBI dye undergoes the formation of molecular aggregates of the J-type in different solvents and adsorbs strongly from aqueous solutions on the glassware, so it may be used as spectral sensitizer in photographic industry. In addition, the quantum chemical calculations have been employed to explain and support the experimental findings. The density functional theory (DFT/B3LYP) and AM1/CI showed that 9-PhEBI has slightly twisted structure which increases upon excitation. The benzothiazolium part is regarded as a strong electron acceptor, while the phenanthryl moiety can be considered as a donor. The orbital topologies reflect the fact that the ICT comes from the phenanthryl subunit to benzothiazolium one via the ethylenic bridge.

References

[1] K. Matsuda, M. Irie, J. Photochem. Photobiol. C: Photochem. Rev. 5 (2004) 169.
[2] M. Irie, Supramol. Sci. 3 (1996) 81, and references their in.
[3] (a) G.M. Tsivgoulis, J.-M. Lehn, Adv. Mater. 9 (1997) 39;
(b) G.M. Tsivgoulis, J.-M. Lehn, Chem. Eur. J. 2 (1996) 1399.
[4] F. Tatezono, T. Harada, Y. Shimizu, M. Ohara, M. Irie, Jpn. J. Appl. Phys. 32 (1993) 3987.
[5] Y. Horikawa, A. Ishikawa, Y. Fujino, M. Hanazawa, K. Ohta, H. Isono, M. Irie, Tech. Dinest ZSOM 94 (1994) 129.
[6] M. Kose, J. Photochem. Photobiol. A: Chem. 165 (2004) 97.
[7] S. Shinkai, T. Nakaji, T. Ogawa, K. Shigematsu, O. Manabe, J. Am. Chem. Soc. 103 (1981) 111.
[8] A. Ueno, H. Yoshimura, R. Saka, T. Osa, J. Am. Chem. Soc. 101 (1979) 2779.
[9] M. Aizawa, K. Nanba, S. Suzuki, Biochim. Biophys. Acta 429 (1976) 975.
[10] M. Montal, Biochim. Biophys. Acta 559 (1979) 231.
[11] T. Kunitake, N. Nakashima, M. Shimomura, Y. Okahata, K. Kano, T. Ogawa, J. Am. Chem. Soc. 102 (1980) 6642.
[12] R.A. Mathies, S.W. Lin, J.B. Ames, W.T. Pollard, Ann. Rev. Biophys. Chem. 20 (1991) 491.
[13] N.C. Maiti, S. Mazumdar, N. Periasamy, J. Phys. Chem. B 102 (1998) 1528.
[14] T. Tani, Photographic Sensitivity: Theory and Mechanisms, Oxford University Press, New York, 1995.
[15] G. Baratocci, U. Mazzucato, A. Spalletti, G. Orlandi, G. Poggi, J. Chem. Soc. Faraday Trans. 2 (88) (1992) 3139.
[16] A. Spalletti, G. Bartocci, G.G. Alosi, Gazz. Chim. Ital. 116 (1986) 705.
[17] B. Juskowiak, M. Chudak, Photochem. Photobiol. 79 (2004) 137.
[18] E.M. Vernigor, V.K. Shalaev, L.P. Novosel'tesva, E.A. Luk'yanets, A.A. Ustenko, V.P. Zvolinskii, V.F. Zakharov, Khim. Geterotsikl. Soedin. 5 (1980) 604.
[19] M. Maus, W. Rettig, D. Bonafoux, R. Lapouyade, J. Phys. Chem. A 103 (1999) 3388.
[20] T.A. Fayed, J. Photochem. Photobiol. A: Chem. 121 (1999) 17.
[21] S.L. Murov, I. Carmichael, G.L. Hug, Handbook of Photochemistry, 2nd ed., Marcel Dekker, New York, 1993.
[22] M.J. Frisch, G.W. Trucks, H.B. Schlegel, G.E. Scuseria, M.A. Robb, J.R. Cheeseman, J.A. Montgomery Jr., T. Vreven, K.N. Kudin, J.C. Burant, J.M. Millam, S.S. Iyengar, J. Tomasi, V. Barone, B. Mennucci, M. Cossi, G. Scalmani, N. Rega, G.A. Petersson, H. Nakatsuji, M. Hada, M. Ehara, K. Toyota, R. Fukuda, J. Hasegawa, M. Ishida, T. Nakajima, Y. Honda, O. Kitao, H. Nakai, M. Klene, X. Li, J.E. Knox, H.P. Hratchian, J.B. Cross, C. Adamo, J. Jaramillo, R. Gomperts, R.E. Stratmann, O. Yazyev, A.J. Austin, R. Cammi, C. Pomelli, J.W. Ochterski, P.Y. Ayala, K. Morokuma, G.A. Voth, P. Salvador, J.J. Dannenberg, V.G. Zakrzewski, S. Dapprich, A.D. Daniels, M.C. Strain, O. Farkas, D.K. Malick, A.D. Rabuck, K. Raghavachari, J.B. Foresman, J.V. Ortiz, Q. Cui, A.G. Baboul, S. Clifford, J. Cioslowski, B.B. Stefanov, G. Liu, A. Liashenko, P. Piskorz, I. Komaromi, R.L. Martin, D.J. Fox, T. Keith, M.A. Al-Laham,

C.Y. Peng, A. Nanayakkara, M. Challacombe, P.M.W. Gill, B. Johnson, W. Chen, M.W. Wong, C. Gonzalez, J.A. Pople, Gaussian 03, Revision D.01, Gaussian, Inc., Wallingford, CT, 2004.
[23] R. Shchepin, D. Litvinov, WinMopac Version 7.21, Semiempirical Calculations Program, Perm State University, Russia, 1998;
D. Takahashi, H. Oda, T. Izumi, R. Hirohashi, Dyes Pigments 66 (2005) 1.
[24] J.E. Leffler, J. Org. Chem. 20 (1955) 1202.
[25] M.D. Green, G. Patonay, T. Ndou, I.M. Warner, Appl. Spectrosc. 46 (1992) 1724.
[26] W. Wu, J. Hua, Y. Jin, W. Zhan, H. Tian, Photochem. Photobiol. Sci. 7 (2008) 63.
[27] E.M. Kosower, J. Am. Chem. Soc. 80 (1958) 5253.
[28] T. Asano, T. Okada, J. Org. Chem. 49 (1984) 4387.
[29] J.H. Espenson, Chemical Kinetics and Reaction Mechanisms, 2nd ed., McGraw-Hill, New York, 1995.